Other investigators[26–28] have reported the measurement of choroidal thickness with the use of OCT at a longer wavelength. In these more recent studies, higher penetration of the OCT probe light, which uses a center wavelength of approximately 1000 nm instead of the current OCT probing light operated at approximately 800 nm, allows the entire choroid to be visualized.[26,27] Swept-source (SS)-OCT at a longer wavelength, which is characterized by a high-speed scan rate and a relatively low sensitivity roll-off versus depth compared with the spectral-domain OCT, obtains a 3-dimensional (3D) high-contrast image of the choroid.[29–34]

In the current study, we scanned the whole macular area of eyes with CSC by high-penetrating SS-OCT using a 3D raster scan protocol and produced a choroidal thickness map of the macular area. By applying both the sectors used by the Early Treatment Diabetic Retinopathy Study (ETDRS) and square grid sectors to this map, we measured the mean choroidal thickness in each area. In addition, we investigated the relationship between choroidal thickness and angiographic changes.

Materials and Methods

All investigations adhered to the tenets of the Declaration of Helsinki, and this prospective study using a prototype of SS-OCT was approved by the institutional review board and the ethics committee at Kyoto University Graduate School of Medicine. Written informed consent was obtained from all participating subjects after the nature and possible consequences of the study were explained.

Subjects

This prospective cross-sectional study enrolled 34 patients (31 men and 3 women; 44 eyes), with CSC but without any other macular abnormality, who visited the Macular Service at Kyoto University Hospital, Kyoto, Japan, between October 2010 and March 2011 and 17 age-matched volunteers (9 men and 8 women; 17 eyes) with no eye disease.

All subjects underwent a comprehensive ophthalmologic examination, including measurement of best-corrected visual acuity and intraocular pressure, autorefractometry/keratometry, indirect ophthalmoscopy, slit-lamp biomicroscopy with a contact lens, color fundus photography, and SS-OCT with a prototype system. All patients with CSC also underwent simultaneous fluorescein angiography (FA) and IA using a confocal laser scanning ophthalmoscope (Heidelberg Retinal Angiograph II; Heidelberg Engineering, Dossenheim, Germany) at the time of SS-OCT measurement. Central serous chorioretinopathy was diagnosed if patients had subretinal fluid involving the macula, as confirmed by OCT, and associated with idiopathic leaks from the RPE during FA, excluding neovascular maculopathy (i.e., age-related macular degeneration, polypoidal choroidal vasculopathy, pathologic myopia, idiopathic choroidal neovascularization, and angioid streaks) and other causes of SRD (i.e., intraocular inflammation, posterior segment tumor, and drusen).

Exclusion criteria for eyes with CSC included history of intraocular surgery, including cataract surgery and photodynamic therapy (PDT), except for retinal photocoagulation; evidence of glaucoma or high intraocular pressure (≥22 mmHg); and poor image due to dense cataract or unstable fixation. Subjects with systemic diseases or conditions that might affect choroidal thickness were also excluded, such as those with diabetes mellitus or malignant hypertension or those who were pregnant.

Exclusion criteria for normal eyes included contraindication to dilation, best-corrected visual acuity <20/25, refractive error of >5.0 or <−6.0 diopters, intraocular pressure of ≥22 mmHg, history of intraocular surgery, evidence of vitreoretinal disease or glaucoma, and poor image due to dense cataract or unstable fixation. Subjects with systemic diseases or conditions that might affect choroidal thickness were also excluded, such as those with diabetes mellitus or malignant hypertension or those who were pregnant.

Classification of Central Serous Chorioretinopathy

Patients with CSC were classified into 3 types: classic CSC, chronic CSC, and multifocal posterior pigment epitheliopathy (MPPE).[35] Classic CSC was defined as 1 or only a few specific points of angiographic leakage from the RPE.[13] Chronic CSC was defined as broad areas of granular hyperfluorescence during FA associated with many indistinct areas of leakage.[13] Multifocal posterior pigment epitheliopathy was defined as multiple massive leakages from the choroid into the subretinal space.[35,36]

All types of CSC eyes were divided into active and resolved eyes. Active eye was defined as SRD involving the macula. Resolved eye was defined by the absence of SRD at the time of SS-OCT measurement. (Resolved eyes included in this study showed active disease at the first visit or the visit before the measurement of SS-OCT and CSC classification [classic, chronic, and MPPE] was based on FA findings in this active phase.)

Unaffected fellow eyes were defined as eyes with no history or evidence of CSC, which was based on the absence of leakage or RPE atrophic changes on FA and no abnormal OCT findings.

Choroidal filling delay was observed in the early phase of IA, and choroidal hyperpermeability and punctate hyperflourescent spots were determined in the late phase of IA. Early-phase IA was studied in 1 eye of each patient; the affected eye was chosen in unilateral CSC, and the eye with active disease was chosen in bilateral CSC. If both eyes were active or resolved, early-phase IA was performed in the eyes with worse visual acuity. All these angiographic features and classifications were evaluated by an experienced ophthalmologist (SO) who was unaware of the SS-OCT results.

Swept-Source Optical Coherence Tomography System and Scan Protocols

We used an SS-OCT prototype system (Topcon, Inc., Tokyo, Japan) with an axial scan rate of 100,000 Hz operated at the 1-μm wavelength region.[34] In the current SS-OCT system, the light source was a wavelength-sweeping laser with a tuning range of approximately 100 nm centered at 1050 nm, yielding 8-μm axial resolution in tissue. Transverse resolution was set to approximately 20 μm. A single OCT image consisting of 1000 A lines can be acquired in 10 ms. The SS-OCT imaging of the cornea was conducted at 1050 nm with approximately 1 mW power, which is well below the safe retinal exposure limit established by the American National Standards Institute. Sensitivity was measured to be approximately 98 dB at this input power.

The SS-OCT examinations were performed by trained examiners after pupil dilation. First, horizontal and vertical line scans (12 mm) through the fovea were obtained, and ~50 B-scan images were averaged to reduce speckle noise. Second, a 3D imaging data set was acquired for each subject with a raster scan protocol of 512 (horizontal) × 128 (vertical) A-scans per data set (total, 65 536 axial scans/volume) in 0.8 seconds. Each 3D scan covered an area of 6×6 mm centered on the fovea, which was confirmed by an

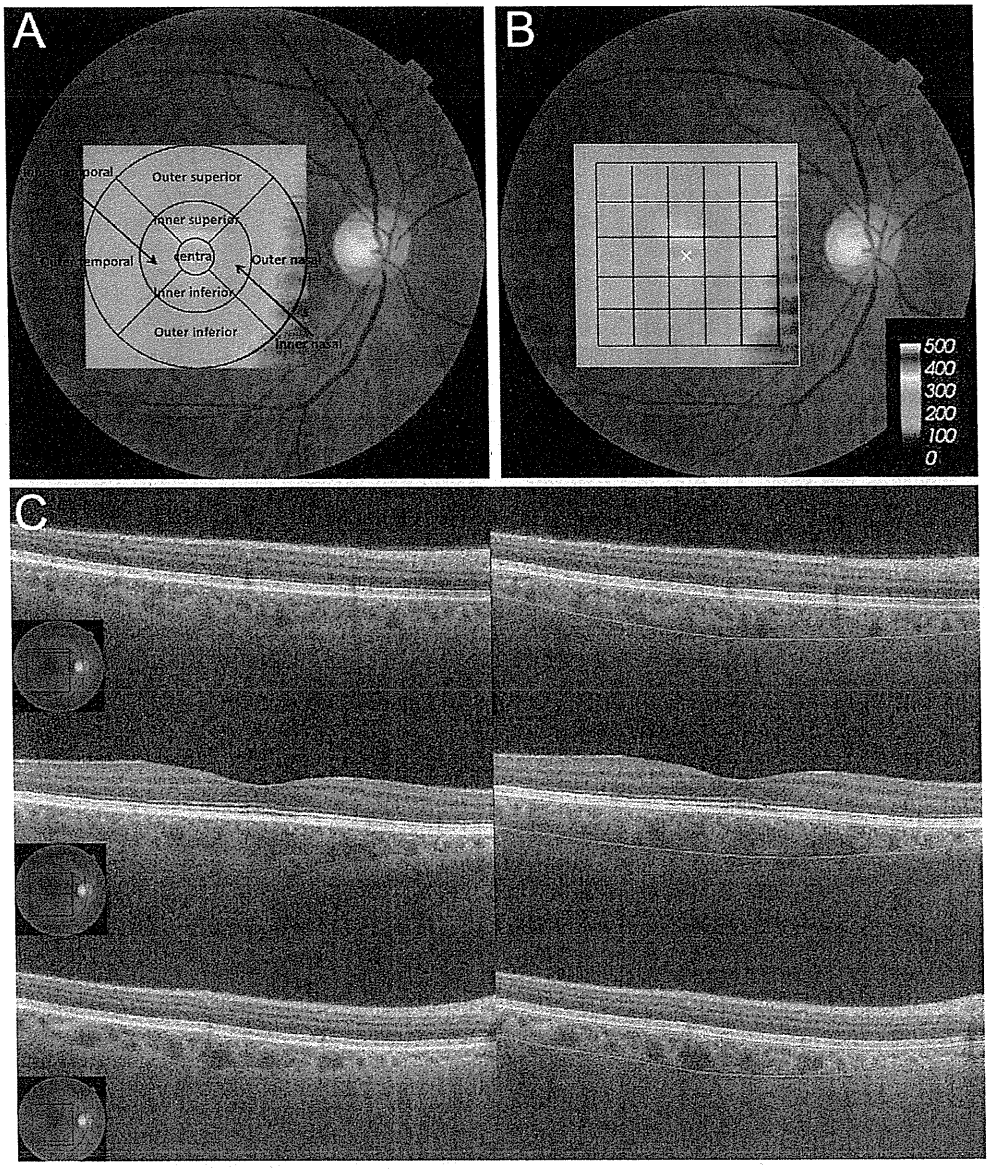

Figure 1. A choroidal thickness map obtained by high-penetrating swept-source optical coherence tomography in a normal eye. **A,** Three-dimensional raster scan covered a 6×6-mm area centered on the fovea. The Early Treatment Diabetic Retinopathy Study sector was applied to the scanned area, and the mean choroidal thickness of 9 sectors was measured. **B,** The 5×5-mm squared grid sector was applied to the scanned area, and the mean choroidal thickness of 25 square areas was measured. **C,** B-scan images at difference levels of the raster scan. *Green lines* indicate the segmentation lines that show Bruch's membrane and the chorioscleral border.

internal-fixation and fundus camera integrated in the instrument. To reduce speckle noise, each image was denoised by applying the weighted moving average from 3 consecutive images.[34] Because of the invisible scanning light and high-speed scanning, eye movement during the 3D scan was minimal.

Choroidal Thickness Measurement

The choroidal thickness was measured as the distance between Bruch's membrane (or the outer border of the RPE-Bruch's membrane complex) and the chorioscleral border (Fig 1). In each image of the 3D data set, both lines were determined manually by a trained ophthalmologist (P.J.) who was blinded to the diagnosis, classification, and angiographic findings. Automated built-in calibration software was used to determine the distance between the 2 lines. From all 128 images of each 3D data set, a choroidal thickness map of 6×6 mm was created. False color was determined starting from a cool color and progressing to a warm color at the range of 0 to 500 μm. After the choroidal thickness map was created, the ETDRS sectors were applied to it (Fig 1A). First, the central fovea on each image was manually registered, if necessary, to coincide with the central circle on the ETDRS segmentation diagram. The mean thickness of each sector was measured in the "center" sector within 0.5 mm from the center of the fovea, in 4 "inner ring" sectors (superior, inferior, nasal, and temporal) 0.5 to 1.5 mm from the center of the fovea, in 4 "outer ring" sectors

Table 1. Mean Age and Refractive Error in Eyes with Each Central Serous Chorioretinopathy (CSC) Subtype

	CSC Eyes								
	Subtype			*Status*					
	Classic (*n* = 23)	*Chronic* (*n* = 17)	*MPPE* (*n* = 4)	*Active* (*n* = 27)	*Resolved* (*n* = 17)	P*	P†	P‡	P§
Patient age (yrs)	53.3±11.5	63.0±14.1	56.5±19.1	58.5±14.3	55.5±14.3	0.067	0.894	0.653	0.485
Refractive error (D)	−1.8±2.8	0.0±1.8	1.5±0.7	−1.1±3.0	−0.4±1.7	0.045	0.035	0.525	0.397

MPPE = multifocal posterior pigment epitheliopathy.
Values are represented as mean ± standard deviation.
*Comparison between classic CSC and chronic CSC by the Turkey–Kramer test.
†Comparison between classic CSC and MPPE by the Turkey–Kramer test.
‡Comparison between chronic CSC and MPPE by the Turkey–Kramer test.
§Comparison between active and resolved CSC by *t* test.

(superior, inferior, temporal, and nasal) 1.5 to 3 mm from the center of the fovea, and as "whole" within 3 mm from the center of the fovea. A 5×5 grid sector of 5×5 mm was further applied to the thickness map. The 5×5 mm grid divided the macular region into 25 square areas (Fig 1B). This grid sector was used for comparison with the angiographic findings. Sectors with angiographic abnormalities, such as choroidal filling delay and choroidal vascular hyperpermeability, were defined as those that involved angiographic abnormalities in more than 50% of the area.

In B-scans where it was difficult to identify the whole outer choroid, 5 to 10 points where the chorioscleral interface could be identified were chosen and connected to create a segmentation line. After creating segmentation lines in all 128 B-scans, the choroidal thickness map was checked. If the thickness differed remarkably between adjoining B-scans, the segmentation lines of the B-scans were rechecked and corrected as required.

Statistical Analyses

A *t* test was used for comparison of variables associated with mean choroidal thickness between normal eyes and eyes with CSC, eyes with unilateral CSC and unaffected fellow eyes, unaffected fellow eyes with and without choroidal hyperpermeability, active eyes and resolved eyes, and areas with angiographic changes and areas without them. A *t* test was also used for a comparison of age and refractive error between normal eyes and CSC eyes and active eyes and resolved eyes. The Tukey–Kramer test was used for comparison of age and refractive error and for comparison of mean choroidal thickness between CSC subtypes. We calculated the Pearson's correlation coefficient and partial correlation to examine associations between choroidal thickness and age or refractive error. All statistical evaluations were performed using commercially available software programs (Dr. SPSS2; SPSS Japan, Tokyo, Japan) (StatMateIII; ATMS, Tokyo, Japan). A *P* value less than 0.05 indicated statistical significance.

Results

In the present study, 34 patients and 17 healthy volunteers were examined. The mean age was 57.3±13.7 years in patients with eyes with CSC and 62.1±15.4 years in patients with normal eyes (P=0.242, *t* test). The mean refractive error was −0.8±2.5 diopters in eyes with CSC and 0.1±2.5 diopters in normal eyes (P=0.245, by the *t* test). Among patients with CSC, 15 had bilateral CSC and 19 had unilateral CSC. However, 5 of the 15 patients with bilateral CSC had a history of PDT in 1 eye, so these 5 eyes were excluded from this study. Thus, 44 eyes of 34 patients with CSC were included, and for 10 patients with bilateral CSC, both eyes were analyzed. (Five patients showed active disease in both eyes, 4 patients showed active disease in 1 eye and resolved disease in 1 eye, and 1 patient showed resolved disease in both eyes.) Twenty-three eyes showed classic CSC (16 eyes showed active disease), 17 eyes showed chronic CSC (8 eyes showed active disease), and 4 eyes had MPPE (3 eyes showed active disease). The mean age and refractive error for each subtype are summarized in Table 1.

Angiographic Data

All patients with CSC were examined using simultaneous FA and IA. Fluorescein angiography showed leakage from the RPE in 25 of 27 active eyes (93%). The area with filling delay in choroidal arteries and choriocapillaris was seen in 20 of 28 eyes (71%). (Early-phase IA images were evaluated in 34 eyes of 34 patients with CSC. However, in 6 eyes, early-phase IA images had undesirable qualities, such as an excessively high intensity; these eyes were excluded from this analysis.)

In late-phase IA, choroidal vascular hyperpermeability was seen in all 44 eyes (100%), and punctuate hyperfluorescent spots were seen in 40 of 44 eyes (91%). In active eyes, choroidal filling delay was observed in 13 of 18 eyes (72%), choroidal hyperpermeability was observed in all 27 eyes (100%), and punctuate hyperfluorescent spots were observed in 25 of 27 eyes (93%). In resolved eyes, choroidal filling delay was observed in 7 of 10 eyes (70%), choroidal hyperpermeability was observed in all 17 eyes (100%), and punctuate hyperfluorescent spots were observed in 15 of 17 eyes (88%).

Macular Choroidal Thickness in Early Treatment Diabetic Retinopathy Study Sectors

The mean choroidal thickness of each ETDRS sector was significantly greater in eyes with CSC compared with normal eyes (Figs 1 and 2, Table 2). Whole macular choroidal thickness in eyes with CSC was 329.3±83.0 μm, which was greater than that in normal eyes (233.0±67.0 μm; $P < 0.001$, *t* test).

In unilateral cases (n = 19), macular choroidal thickness was greater in 8 of 9 sectors in affected eyes than in unaffected fellow eyes (Table 3). The whole macular choroidal thickness was greater in eyes with unilateral CSC (326.6±98.4 μm) than in unaffected fellow eyes (254.2±86.8 μm; $P = 0.021$, *t* test).

The whole macular choroidal thickness did not differ between unaffected fellow eyes (n = 19; 254.2±86.8 μm) and normal eyes (233.0±67.0 μm; $P = 0.423$, *t* test). The whole macular choroidal

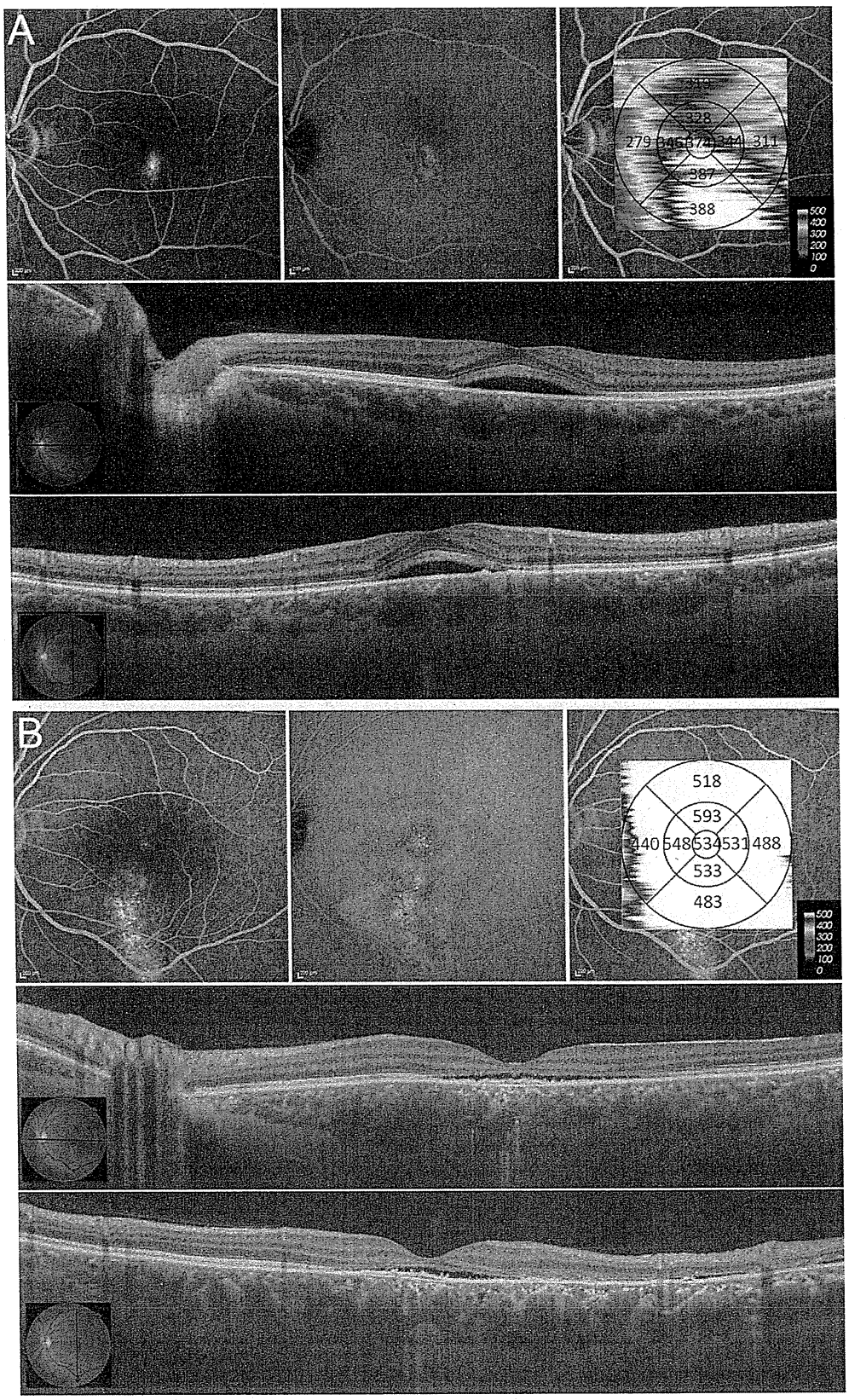

Figure 2.

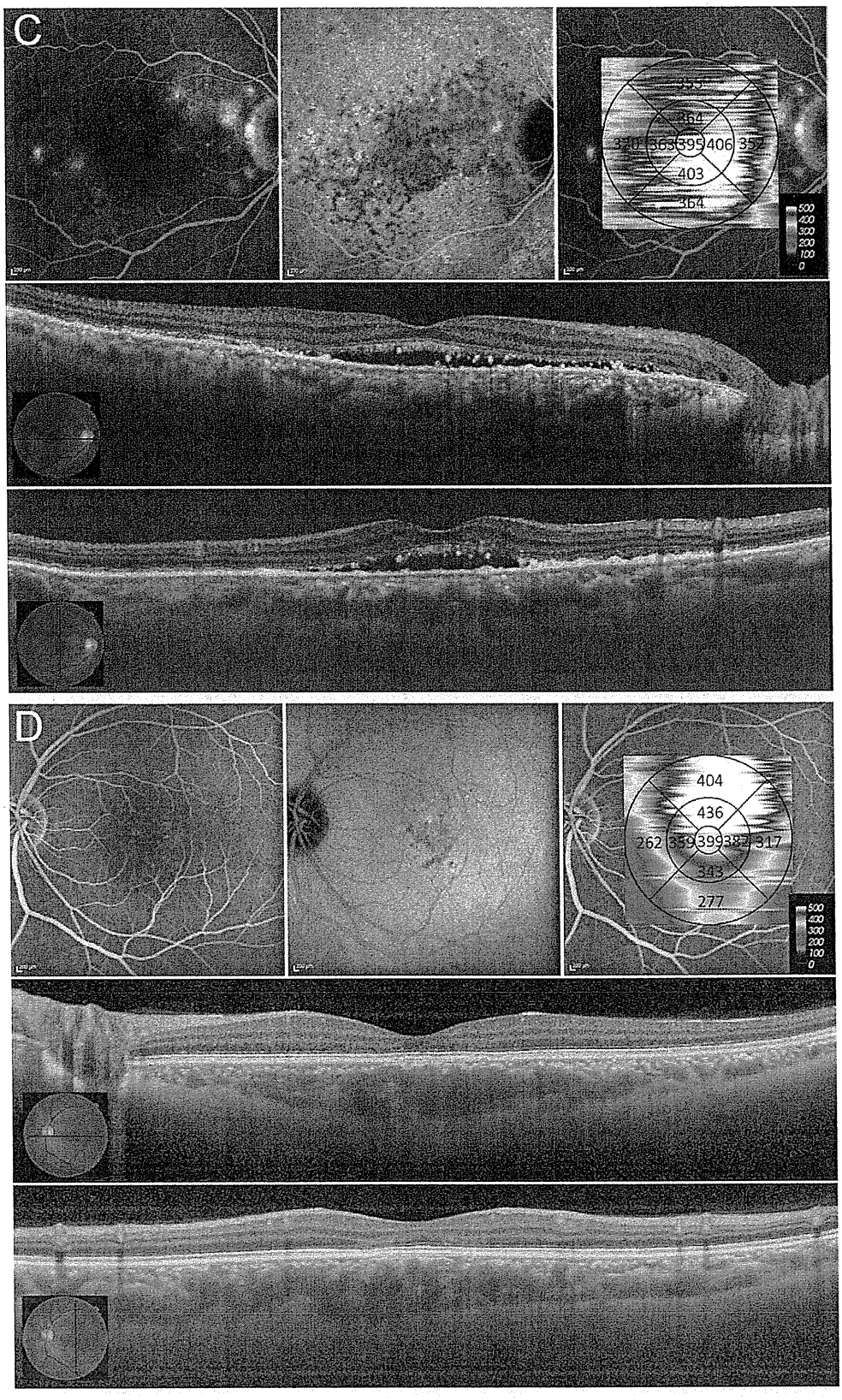

Figure 2. *(Continued.)*

Table 2. Mean Choroidal Thickness in Eyes with Central Serous Chorioretinopathy (CSC) and in Normal Eyes

Area (μm)	CSC (n = 44)	Normal Eyes (n = 17)	P*
Whole macula	329.3±83.0	233.0±67.0	<0.001
Center	374.3±92.9	248.4±77.4	<0.001
Inner temporal	366.5±91.5	247.4±76.8	<0.001
Inner superior	363.2±92.9	250.4±73.4	<0.001
Inner nasal	352.7±96.1	229.6±77.6	<0.001
Inner inferior	360.1±93.4	246.3±72.7	<0.001
Outer temporal	327.2±83.0	237.6±72.3	<0.001
Outer superior	333.5±88.0	261.9±67.2	0.004
Outer nasal	285.7±91.3	189.0±70.3	<0.001
Outer inferior	326.9±82.7	228.8±68.6	<0.001

Values are represented as mean ± standard deviation.
Inner, 0.5–1.5 mm from foveal center; outer, 1.5–3 mm from the foveal center.
*Comparison between CSC and normal eyes by *t* test.

thickness of the unaffected fellow eyes with choroidal hyperpermeability (n = 11; 273.4±86.6 μm) was slightly increased compared with eyes without choroidal hyperpermeability (n = 8; 227.6±85.3 μm) or normal eyes (n = 17; 233.0±67.0 μm), but the difference was not significant ($P = 0.268$ and $P = 0.176$, respectively, *t* test).

There was no significant difference between choroidal thickness in active eyes and resolved eyes in each ETDRS sector (Table 4, available at http://aaojournal.org). The mean whole macular choroidal thickness was 342.2±75.9 μm in active eyes and 308.8±91.7 μm in resolved eyes ($P = 0.196$ by *t* test). The mean whole macular choroidal thickness was more in eyes (n = 7) that had undergone laser photocoagulation than in eyes (n = 37) that had not (395.0±74.1 μm and 316.8±79.4 μm, respectively; $P = 0.020$, *t* test).

The mean choroidal thickness of each area in the ETDRS showed no significant difference among classic CSC, chronic CSC, and MPPE; however, all of them showed increased thickness compared with normal eyes (Figs 1 and 2, Table 5). The mean whole macular choroidal thickness was 326.9±83.1 μm in cases of classic CSC, 325.4±93.3 μm in chronic CSC, and 359.0±15.5 μm in MPPE, which were greater than in normal eyes ($P < 0.001$, $P = 0.002$, $P=0.002$, respectively, *t* test).

In active eyes, the mean choroidal thickness of each ETDRS sector showed no significant difference among classic CSC, chronic CSC, and MPPE. The mean whole macular choroidal thickness was 341.9±72.9 μm in classic CSC, 339.0±99.7 μm in chronic CSC, and 352.0±8.0 μm in MPPE. In resolved eyes, the mean choroidal thickness of each ETDRS sector showed no significant difference between classic CSC and chronic CSC. The mean whole macular choroidal thickness was 292.7±100.1 μm for classic CSC and 313.4±91.2 μm for chronic CSC.

A significant difference was found in the refractive error among eyes with classic CSC, chronic CSC, and MPPE. Therefore, we analyzed only CSC eyes with a refractive error of ±1.5 diopters. The mean choroidal thickness of each ETDRS sector showed no significant differences among the 3 disease subtypes (Table 6, available at http://aaojournal.org).

Choroidal Thickness and Angiographic Changes

The relationship between the mean choroidal thickness in each 5×5 grid sector and the angiographic findings were evaluated (Figs 3 and 4; Table 7). Sectors with angiographic abnormalities such as choroidal filling delay and hyperpermeability were defined as those that involved more than 50% of the sector area. Choroidal thickness was greater in areas with leakage on FA (361.9±81.5 μm) than in areas without leakage (337.6±81.5 μm; $P=0.001$, *t* test). Choroidal thickness was greater in areas with choroidal vascular hyperpermeability on IA (356.8±92.7 μm) than in unaffected areas (319.4±90.7 μm; $P < 0.001$, *t* test). In addition, choroidal thickness was greater in areas with punctate hyperfluorescent spots on IA (367.6±87.9 μm) than in unaffected areas (333.8±87.9 μm; $P < 0.001$, *t* test). However, choroidal thickness did not differ between areas with choroidal filling delay and areas without it ($P = 0.872$, *t* test).

Correlation among Age, Refractive Error, and Choroidal Thickness in Eyes with Central Serous Chorioretinopathy

Table 8 (available at http://aaojournal.org) shows Pearson's correlation coefficient and partial correlation coefficient between macular choroidal thickness and age or refractive error. The whole macular choroidal thickness was correlated significantly with age after adjusting for refractive error ($r = -0.477$; $P = 0.001$) and with refractive error after adjusting for age ($r = 0.366$; $P = 0.016$).

Discussion

Although the pathophysiology of CSC remains unknown, there is strong angiographic evidence that the key underlying mechanism involves choroidal vascular abnormalities. Studies using IA have shown a variety of choroidal abnormalities in patients with CSC, including variable filling

Figure 2. Macular choroidal thickness in each subtype of central serous chorioretinopathy (CSC). **A,** Active classic CSC. Fluorescein angiography shows an ink blot pattern of leakage (*top, left*); indocyanine green angiography (IA) shows choroidal hyperpermeability and punctate hyperfluorescent spots (*top, middle*); choroidal thickness map shows increased choroidal thickness in the whole macula (*top, right*). The swept-source optical coherence tomography (SS-OCT) images (12 mm) of the fovea show serous retinal detachment (SRD) and a thick choroid (*second row, bottom*). **B,** Active chronic CSC. Fluorescein angiography shows broad areas of granular hyperfluorescence associated with many indistinct areas of leakage (*top, left*); IA shows choroidal hyperpermeability and punctuate hyperfluorescent spots (*top, middle*); choroidal thickness map shows increased choroidal thickness in the whole macula (*top, right*). The SS-OCT images through the fovea show SRD, thin central retina, and a thick choroid (*second row, bottom*). **C,** Active multifocal posterior pigment epitheliopathy. Fluorescein angiography shows multiple massive leakages (*top, left*); IA shows several areas of choroidal hyperpermeability and punctuate hyperfluorescent spots (*top, middle*); choroidal thickness map shows increased choroidal thickness in the whole macula (*top, right*). The SS-OCT images through the fovea show SRD and a thick choroid (*second row, bottom*). **D,** Resolved classic CSC. Fluorescein angiography shows a window defect and no remarkable leakage (*top, left*); IA shows several areas of choroidal hyperpermeability and punctuate hyperfluorescent spots (*top, middle*); choroidal thickness map shows increased choroidal thickness in the whole macula (*top, right*). The SS-OCT images through the fovea show no SRD but do show the presence of a thick choroid (*second row, bottom*).

Table 3. Mean Choroidal Thickness in Eyes with Unilateral Central Serous Chorioretinopathy (CSC) and in Unaffected Fellow Eyes

Area (μm)	Unilateral CSC Eyes (n = 19)	Unaffected Fellow Eyes (n = 19)	P*
Whole macula	326.6±98.4	254.2±86.8	0.021
Center	376.5±115.2	287.6±101.6	0.016
Inner temporal	373.0±116.8	286.0±98.3	0.018
Inner superior	353.7±110.7	275.8±89.4	0.022
Inner nasal	348.3±112.8	260.4±98.0	0.015
Inner inferior	368.5±112.2	269.0±100.8	0.007
Outer temporal	330.5±104.6	263.2±86.7	0.038
Outer superior	322.3±96.8	265.1±84.5	0.060
Outer nasal	275.3±108.1	206.9±89.0	0.040
Outer inferior	330.1±92.9	254.4±86.8	0.014

Values are represented as mean ± standard deviation.
Inner, 0.5–1.5 mm from the foveal center; outer, 1.5–3 mm from the central fovea.
*Comparison between unilateral CSC eyes and unaffected fellow eyes by *t* test.

delay in the regions within the choroid,[2–6] choroidal venous dilation,[2,4,5] multiple areas of choroidal vascular hyperpermeability,[1–17] and punctate choroidal hyperfluorescent spots,[14] suggesting that a generalized choroidal vascular disturbance occurs in CSC. Other studies have shown evidence of hyperdynamic circulation within the choroid in eyes with CSC.[37,38]

Imamura et al[18] reported that EDI-OCT demonstrated the presence of a thick choroid in patients with CSC. On the other hand, Maruko et al[19] reported that focal laser photocoagulation did not result in any change in choroidal thickness with the use of EDI-OCT, whereas PDT led to choroidal thinning and decreased hyperpermeability seen during IA in eyes with CSC. However, in the studies using EDI-OCT, choroidal thickness measurements were indicated by a representative value obtained at several points, such as the foveal center and at 500-μm increments from the fovea. This measurement tends to be influenced by focal thickening or thinning of the choroid or, more often, with irregularity of the choriosclera border. In the current study, by using 3D raster scanning images obtained by high-penetrating SS-OCT, eyes with CSC were found to have thickened choroids in the whole macular area and focally increased choroidal thickness associated with angiographic findings.

Several investigators have reported that foveal choroidal thickness is correlated with age, axial length, or refractive error in normal subjects.[16,34,39] We also found that the mean macular choroidal thickness had a negative correlation with age and refractive error in eyes with CSC. These results suggest that both age and refractive error should be considered in measuring choroidal thickness even in pathologic eyes. In the current study, age- and refractive error–matched normal controls were used, and explorative analysis was also performed when a difference was found in age or refractive error in eyes with CSC subtypes.

Central macular choroidal thickness in eyes with CSC was greater than that in normal eyes, which is consistent with the results of Imamura et al[18] and Maruko et al.[20] In addition, choroidal thickness in the whole macular area and in each ETDRS sector area was found to be increased in eyes with CSC. This result corresponds to the finding that choroidal abnormalities on IA are not only confined to the fovea but also extend into other areas of the macula. Moreover, the central choroidal thickness in unilateral symptomatic eyes was greater than in the unaffected fellow eyes in most of ETDRS sectors. Maruko et al[20] reported that the subfoveal choroidal thickness in unilateral symptomatic eyes was greater than that in fellow eyes, which is consistent with our study. They also showed that subfoveal choroidal thickness was greater in unaffected fellow eyes than in age-matched normal eyes and greater in unaffected eyes

Table 5. Mean Choroidal Thickness in Each Subtype of Central Serous Chorioretinopathy (CSC) versus Normal Eyes

	CSC Subtype						
Area (μm)	*Classic* (*n* = 23)	*Chronic* (*n* = 17)	*MPPE* (*n* = 4)	Normal Eyes (n = 17)	P*	P†	P‡
Whole macula	326.9±83.1	325.4±93.3	359.0±15.5	233.0±67.0	<0.001	0.002	0.002
Center	374.2±94.9	368.7±103.0	398.7±17.1	248.4±77.4	<0.001	0.001	0.001
Inner temporal	365.0±94.8	368.2±100.4	367.9±17.6	247.4±76.8	<0.001	<0.001	0.006
Inner superior	360.5±96.0	362.2±101.9	382.6±16.9	250.4±73.4	<0.001	0.001	0.002
Inner nasal	346.7±94.0	350.3±110.0	396.9±15.9	229.6±77.6	<0.001	0.001	<0.001
Inner inferior	354.1±90.7	361.6±108.8	387.7±17.3	246.3±72.7	<0.001	0.001	0.001
Outer temporal	327.1±86.6	326.5±90.3	331.2±16.9	237.6±72.3	0.001	0.003	0.021
Outer superior	338.9±89.3	317.7±95.6	369.6±17.5	261.9±67.2	0.005	0.058	0.006
Outer nasal	277.2±89.7	283.2±101.3	344.9±23.6	189.0±70.3	0.002	0.004	<0.001
Outer inferior	322.0±80.8	326.3±95.0	355.2±25.9	228.8±68.6	<0.001	0.002	0.002

MPPE = multifocal posterior pigment epitheliopathy.
Values are mean ± SD.
Inner = 0.5–1.5 mm from foveal center; outer = 1.5–3 mm from central fovea.
*Comparison between classic CSC and normal eyes by *t* test.
†Comparison between chronic CSC and normal eyes by *t* test.
‡Comparison between MPPE and normal eyes by *t* test.

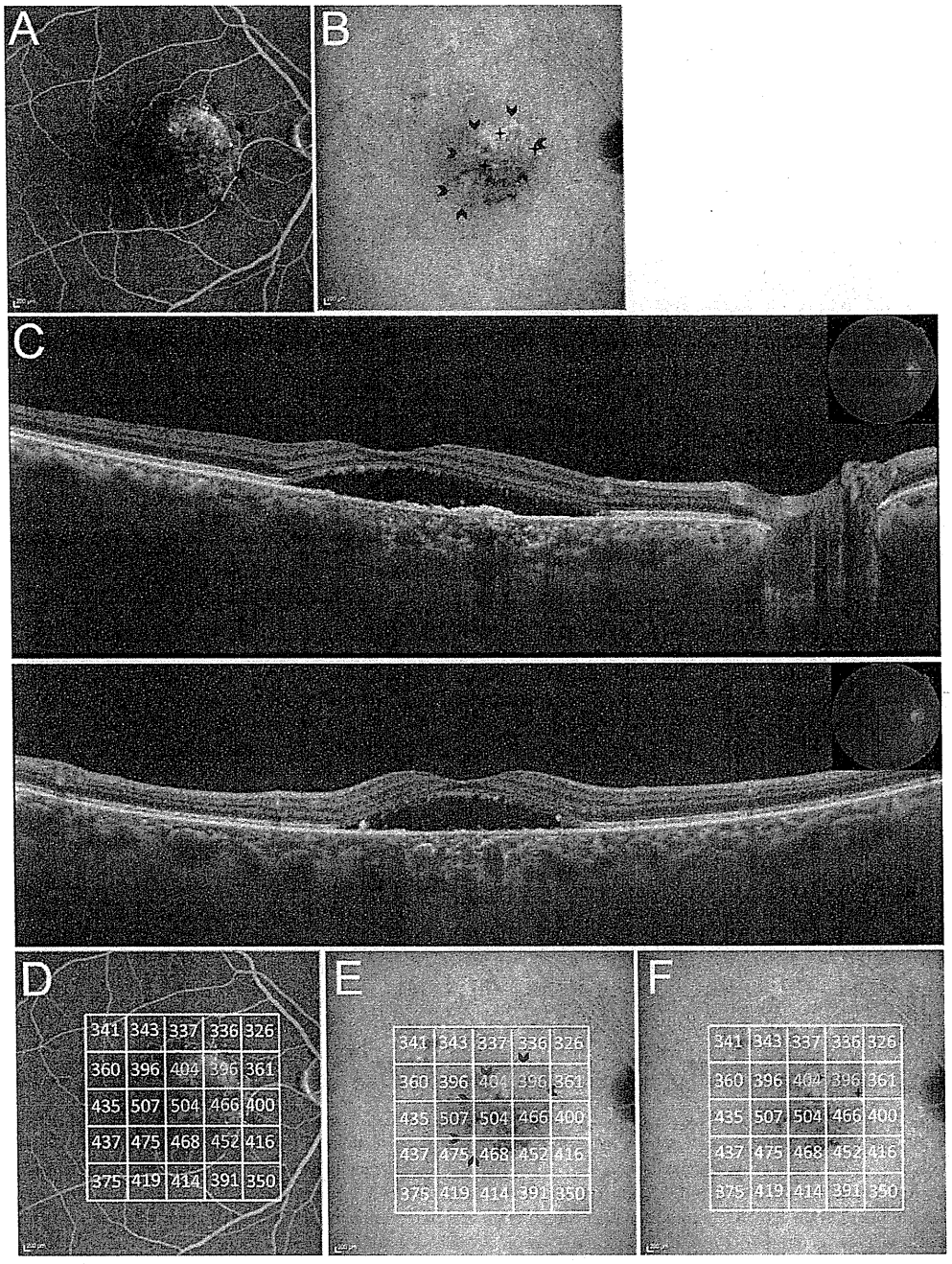

Figure 3. Comparison of the mean choroidal thickness and angiographic findings in an eye with active chronic central serous chorioretinopathy. **A,** Fluorescein angiography (FA) shows diffuse leakage (*red triangles*). **B,** Late-phase indocyanine green angiography shows choroidal hyperpermeability (*red arrowheads*) and punctate hyperfluorescent spots (*blue stars*). **C,** The swept-source optical coherence tomography images show serous retinal detachment in the fovea and a thick choroid. **D,** The mean choroidal thickness in areas with FA leakage indicted by *red* (442.5 μm) was greater compared with non-FA leakage areas (397.1 μm). **E,** The mean choroidal thickness in areas with choroidal hyperpermeability indicated by *red* (458.7 μm) was greater compared with the nonhyperpermeability areas (387.2 μm). **F,** The mean choroidal thickness in areas with punctuate hyperfluorescent spots indicated by *red* (434.7 μm) was greater compared with nonpunctate hyperfluorescent areas (400.2 μm).

with choroidal vascular hyperpermeability than in unaffected eyes without choroidal vascular hyperpermeabilty. Our subjects showed a similar tendency, but the results were not statistically significant, probably because of the small sample size.

There was no significant difference in the choroidal thickness between active eyes and resolved eyes. These findings suggest that choroidal thickness is increased in patients with CSC regardless of the resolution of SRD. In addition, Iida et al[5] found that choroidal vascular abnor-

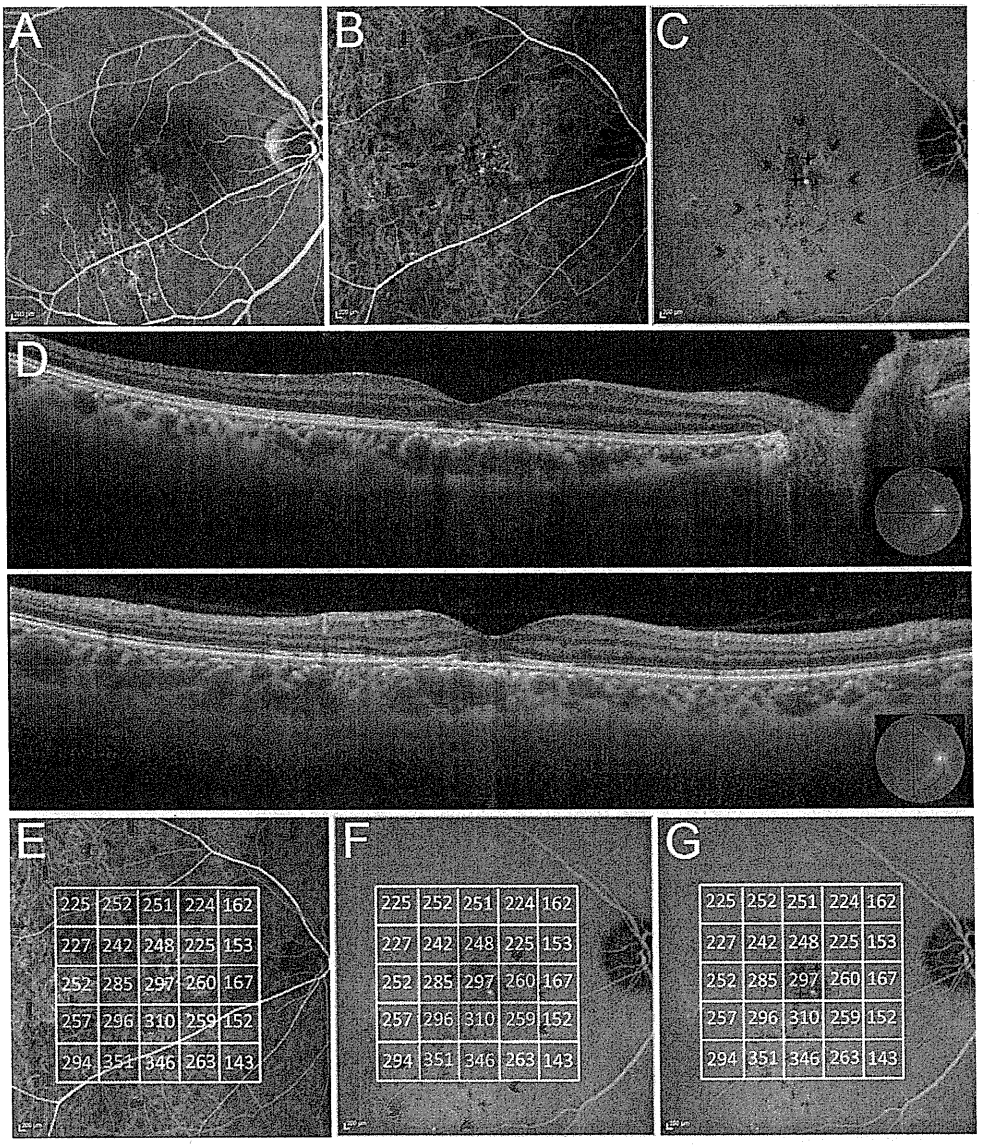

Figure 4. Comparison of the mean choroidal thickness and angiographic findings in an eye with resolved chronic central serous chorioretinopathy. **A,** Fluorescein angiography shows a window defect in an area with retinal pigment epithelium alteration and no remarkable leakage. **B,** Early-phase indocyanine green angiography (IA) shows filling delay in choroidal arteries and choriocapillaris (*red arrows*). **C,** Late-phase IA shows choroidal hyperpermeability (*red arrowheads*) and punctate hyperfluorescent spots (*blue stars*). **D,** The swept-source optical coherence tomography images show no serous retinal detachment but do show a thick choroid. **E,** The mean choroidal thickness in areas with filling delay indicated by *red* (247.1 μm) was almost equal to that in nonfilling delayed areas (243.5 μm). **F,** The mean choroidal thickness in areas with choroidal hyperpermeability indicated by *red* (302.7 μm) was greater than that in nonhyperpermeability areas (223.4 μm). **G,** The mean choroidal thickness in areas with punctuate hyperfluorescent spots indicated by *red* (303.5 μm) was greater than that in nonpunctate hyperfluorescent areas (240.6 μm).

malities in IA persist in both eyes even after the cessation of leakage from the RPE. Thus, choroidal structural abnormalities may persist even after the resolution of SRD. These findings may have a relationship with the well-known phenomenon that SRD tends to recur, especially in areas with choroidal hyperpermeability, in patients with CSC.[5,10,11]

In a longitudinal study, Maruko et al[19] reported that focal laser photocoagulation did not result in any change in choroidal thickness, although SRD was decreased. In the current cross-sectional study, the mean choroidal thickness of eyes with a history of laser photocoagulation was greater than that of eyes without photocoagulation treatment. Taken together, it seems that laser photocoagulation therapy does not result in a decrease in choroidal thickness but just covers the leakage from RPE.

Some patients with CSC have shown recent onset of the disease with 1 or only a few specific points of leakage from the RPE; these eyes are commonly termed as having "classic CSC."[13] Other patients with chronic disease have

Table 7. Mean Choroidal Thickness in Areas with Angiographic Abnormalities versus Areas without Angiographic Abnormalities

Area (μm)	Affected Area	Unaffected Area	P*
FA leakage	361.9±81.5	337.6±81.5	0.001
Choroidal filling delay	339.1±100.3	340.6±93.9	0.872
Choroidal hyperpermeability	356.8±92.7	319.4±90.7	<0.001
Punctuate hyperfluorescent spots	367.6±87.9	333.8±87.9	<0.001

FA = fluorescence angiography.
Values are represented as mean ± standard deviation.
*Comparison between affected and unaffected area by *t* test.

broad areas of granular hyperfluorescence during FA, which are associated with many indistinct areas of leakage. These patients have chronic CSC, which has also been called "diffuse retinal pigment epitheliopathy."[8,13,19] A type of exudative retinal detachment, usually manifested with flat SRD in the posterior pole and bullous retinal detachment in the lower periphery, was reported as bullous retinal detachment in 1973[36] and termed "MPPE" in 1999.[35] Multifocal posterior pigment epitheliopathy has been considered an unusual manifestation and severe form of CSC.[35] In the current study, all eyes of these types showed choroidal hyperpermeability, and choroidal thickness was equally increased in classic CSC, chronic CSC, and MPPE. The underlying IA abnormality unifying them is choroidal vascular hyperpermeability, and the underlying OCT finding unifying them is increased choroidal thickness. Thus, classic CSC, chronic CSC, and MPPE may share a common pathology with choroidal vascular abnormalities, although the visual prognosis is different.

Choroidal thickness was greater in the area with leakage points on FA than in the area without it. Moreover, choroidal thickness was greater in the area with choroidal hyperpermeability on IA than in the unaffected areas. An increase in hydrostatic pressure within the choroid sufficient to cause changes to the overlying RPE and retina may cause structural changes within the choroid itself. Focal thickening of the choroid in these areas may suggest that focal hydrostatic pressure within the choroid is increased in the area with choroidal vascular hyperpermeability, resulting in pigment epithelial detachment with subsequent RPE defect,[40] which in turn results in focal leakage into the subretinal space. In addition, choroidal thickness was greater in areas with punctate hyperfluorescent spots on IA than in unaffected areas. Punctate hyperfluorescent spots have been reported to be located in the inner choroid and seen at the center of the focal hyperfluorescent area on IA. This area often expands from the punctate spots,[14] possibly resulting in increased pressure in the inner choroid or Bruch's membrane and leading to a break in the barrier of RPE. Thus, focal increased choroidal thickness in the area with punctate lesions may be explained by increased pressure in the inner choroid.

Ikuno et al[41] investigated the agreement among choroidal thickness parameters measured using high-penetration SS-OCT and commercially available spectral domain-OCT with the EDI technique; they reported that choroidal thickness was well correlated between these instruments.[41] Thus, similar outcomes could have been obtained if spectral domain-OCT was used in the present study. However, EDI-OCT is usually coupled to multiple averaging to achieve high contrast and low speckle noise. This results in smaller numbers of B-scan images than 3D raster scan images, and interpolation is required to fill in the nonimaged areas. This sparse sampling density may be inadequate, especially for the assessment of extrafoveal choroidal thickness and angiographic changes.

There are some limitations to this study. Although the high-penetrating SS-OCT increases the sensitivity of the choroid, scattering of light by the RPE and choroid still occurs, which makes visualization of the chorioscleral interface difficult in some patients, especially in eyes with thick choroid. There is currently no automated segmentation software available for measuring choroidal thickness; thus, we performed all segmentations manually. However, we have previously shown good interobserver repeatability with this technique.[34]

In conclusion, we demonstrated that choroidal thickness was increased in the whole macular area in all types of CSC and that choroidal thickness was associated with leakage from the RPE, choroidal vascular hyperpermeability, and punctate hyperfluorescent lesions. These findings provide the evidence that CSC may be caused by focally increased hydrostatic pressure in the choroid.

References

1. Guyer DR, Yannuzzi LA, Slakter JS, et al. Digital indocyanine green videoangiography of central serous chorioretinopathy. Arch Ophthalmol 1994;112:1057–62.
2. Menchini U, Virgili G, Lanzetta P, Ferrari E. Indocyanine green angiography in central serous chorioretinopathy: ICG angiography in CSC. Int Ophthalmol 1997;21:57–69.
3. Prunte C. Indocyanine green angiographic findings in central serous chorioretinopathy. Int Ophthalmol 1995;19:77–82.
4. Prunte C, Flammer J. Choroidal capillary and venous congestion in central serous chorioretinopathy. Am J Ophthalmol 1996;121:26–34.
5. Iida T, Kishi S, Hagimura N, Shimizu K. Persistence and bilateral choroidal vascular abnormalities in central serous chorioretinopathy. Retina 1999;19:508–12.
6. Kitaya N, Nagaoka T, Hikichi T, et al. Features of abnormal choroidal circulation in central serous chorioretinopathy. Br J Ophthalmol 2003;87:709–12.
7. Spaide RF, Goldbaum M, Wong DW, et al. Serous detachment of the retina. Retina 2003;23:820–46.
8. Spaide RF, Hall L, Haas A, et al. Indocyanine green videoangiography of older patients with central serous chorioretinopathy. Retina 1996;16:203–13.
9. Spaide RF, Campeas L, Haas A, et al. Central serous chorioretinopathy in younger and older adults. Ophthalmology 1996;103:2070–9.
10. Piccolino FC, Borgia L. Central serous chorioretinopathy and indocyanine green angiography. Retina 1994;14:231–42.

11. Piccolino FC, Borgia L, Zinicola E, Zingirian M. Indocyanine green angiographic findings in central serous chorioretinopathy. Eye (Lond) 1995;9:324–32.
12. Scheider A, Nasemann JE, Lund OE. Fluorescein and indocyanine green angiographies of central serous choroidopathy by scanning laser ophthalmoscopy. Am J Ophthalmol 1993; 115:50–6.
13. Klais CM, Ober MD, Ciardella AP, Yannuzzi LA. Central serous chorioretinopathy. In: Ryan SJ, ed-in-chief, Hinton DR, Schachat AP, Wilkinson CP, eds. Retina. 4th ed. vol. 2. Philadelphia, PA: Elsevier/Mosby; 2006:1135–61.
14. Tsujikawa A, Ojima Y, Yamashiro K, et al. Punctate hyperfluorescent spots associated with central serous chorioretinopathy as seen on indocyanine green angiography. Retina 2010;30:801–9.
15. Spaide RF, Koizumi H, Pozzoni MC. Enhanced depth imaging spectral-domain optical coherence tomography. Am J Ophthalmol 2008;146:496–500.
16. Margolis R, Spaide RF. A pilot study of enhanced depth imaging optical coherence tomography of the choroid in normal eyes. Am J Ophthalmol 2009;147:811–5.
17. Doro D, Visentin S, Maimone PE, Pilotto E. High-resolution ultrasonography in central serous chorioretinopathy. Am J Ophthalmol 2005;139:550–2.
18. Imamura Y, Fujiwara, T, Margolis R, Spaide RF. Enhanced depth imaging optical coherence tomography of the choroid in central serous chorioretinopathy. Retina 2009;29:1469–73.
19. Maruko I, Iida T, Sugano Y, et al. Subfoveal choroidal thickness after treatment of central serous chorioretinopathy. Ophthalmology 2010;117:1792–9.
20. Maruko I, Iida T, Sugano Y, et al. Subfoveal choroidal thickness in fellow eyes of patients with central serous chorioretinopathy. Retina 2011;31:1603–8.
21. Spaide RF. Enhanced depth imaging optical coherence tomography of retinal pigment epithelial detachment in age-related macular degeneration. Am J Ophthalmol 2009;147:644–52.
22. Reibaldi M, Boscia F, Avitabile T, et al. Enhanced depth imaging optical coherence tomography of the choroid in idiopathic macular hole: a cross-sectional prospective study. Am J Ophthalmol 2011;151:112–7.
23. Chung SE, Kang SW, Lee JH, Kim YT. Choroidal thickness in polypoidal choroidal vasculopathy and exudative age-related macular degeneration. Ophthalmology 2011;118:840–5.
24. Maruko I, Iida T, Sugano Y, et al. Subfoveal choroidal thickness after treatment of Vogt-Koyanagi-Harada disease. Retina 2011;31:510–7.
25. Maruko I, Iida T, Sugano Y, et al. Subfoveal retinal and choroidal thickness after verteporfin photodynamic therapy for polypoidal choroidal vasculopathy. Am J Ophthalmol 2011; 151:594–603.
26. Esmaeelpour M, Povazay B, Hermann B, et al. Three-dimensional 1060-nm OCT: choroidal thickness maps in normal subjects and improved posterior segment visualization in cataract patients. Invest Ophthalmol Vis Sci 2010;51:5260–6.
27. Povazay B, Bizheva K, Hermann B, et al. Enhanced visualization of choroidal vessels using ultrahigh resolution ophthalmic OCT at 1050 nm. Opt Express [serial online] 2003;11: 1980–6. Available at: http://www.opticsinfobase.org/abstract.cfm?URI=oe-11-17-1980. Accessed February 11, 2012.
28. Huber R, Adler DC, Srinivasan VJ, Fujimoto JG. Fourier domain mode locking at 1050 nm for ultra-high-speed optical coherence tomography of the human retina at 236,000 axial scans per second. Opt Lett 2007;32:2049–51.
29. de Bruin DM, Burnes DL, Loewenstein J, et al. In vivo three-dimensional imaging of neovascular age-related macular degeneration using optical frequency domain imaging at 1050 nm. Invest Ophthalmol Vis Sci 2008;49:4545–52.
30. Potsaid B, Baumann B, Huang D, et al. Ultrahigh speed 1050nm swept source/Fourier domain OCT retinal and anterior segment imaging at 100,000 to 400,000 axial scans per second. Opt Express [serial online] 2010;18:20029–48. Available at: http://www.opticsinfobase.org/abstract.cfm?URI=oe-18-19-20029. Accessed February 11, 2012.
31. Srinivasan VJ, Huber R, Gorczynska I, et al. High-speed, high-resolution optical coherence tomography retinal imaging with a frequency-swept laser at 850 nm. Opt Lett 2007;32: 361–3.
32. Unterhuber A, Povazay B, Hermann B, et al. In vivo retinal optical coherence tomography at 1040 nm - enhanced penetration into the choroid. Opt Express [serial online] 2005;13: 3252–8. Available at: http://www.opticsinfobase.org/abstract.cfm?URI=oe-13-9-3252. Accessed February 11, 2012.
33. Yasuno Y, Hong Y, Makita S, et al. In vivo high-contrast imaging of deep posterior eye by 1-micron swept source optical coherence tomography and scattering optical coherence angiography. Opt Express [serial online] 2007;15:6121–39. Available at: http://www.opticsinfobase.org/abstract.cfm?URI=oe-15-10-6121. Accessed February 11, 2012.
34. Hirata M, Tsujikawa A, Matsumoto A, et al. Macular choroidal thickness and volume in normal subjects measured by swept-source optical coherence tomography. Invest Ophthalmol Vis Sci 2011:52:4971–8.
35. Uyama M, Matsunaga H, Matsubara T, et al. Indocyanine green angiography and pathophysiology of multifocal posterior pigment epitheliopathy. Retina 1999;19:12–21.
36. Gass JD. Bullous retinal detachment: an unusual manifestation of idiopathic central serous choroidopathy. Am J Ophthalmol 1973;75:810–21.
37. Tittl M, Polska E, Kircher K, et al. Topical fundus pulsation measurement in patients with active central serous chorioretinopathy. Arch Ophthalmol 2003;121:975–8.
38. Tittl M, Maar N, Polska E, et al. Choroidal hemodynamic changes during isometric exercise in patients with inactive central serous chorioretinopathy. Invest Ophthalmol Vis Sci 2005;46:4717–21.
39. Ikuno Y, Kawaguchi K, Nouchi T, Yasuno Y. Choroidal thickness in healthy Japanese subjects. Invest Ophthalmol Vis Sci 2010;51:2173–6.
40. Fujimoto H, Gomi F, Wakabayashi T, et al. Morphologic changes in acute central serous chorioretinopathy evaluated by Fourier-domain optical coherence tomography. Ophthalmology 2008;115:1494–500.
41. Ikuno Y, Maruko I, Yasuno Y, et al. Reproducibility of retinal and choroidal thickness measurements in enhanced depth imaging and high-penetration optical coherence tomography. Invest Ophthalmol Vis Sci 2011;52:5536–40.

Footnotes and Financial Disclosures

Originally received: September 30, 2011.
Final revision: January 12, 2012.
Accepted: February 15, 2012.
Available online: ●●●. Manuscript no. 2011-1443.

[1] Department of Ophthalmology and Visual Sciences, Kyoto University Graduate School of Medicine, Kyoto, Japan.

[2] Department of Ophthalmology, Faculty of Medicine, Prince of Songkla University, Songkhla, Thailand.

[3] Topcon Corporation, Tokyo, Japan.

Financial Disclosure(s):
The author(s) have made the following disclosure(s): Masanori Hangai and Nagahisa Yoshimura are paid members of the advisory boards of Topcon Inc., and Akiko Matsumoto is an employee of Topcon Inc.

Funding: This research was partially supported by a Grant-in-Aid for Scientific Research (21796179) from the Japan Society for the Promotion of Science (JSPS) and Topcon Inc. (Tokyo, Japan).

Correspondence:
Sotaro Ooto, MD, Department of Ophthalmology and Visual Sciences, Kyoto University Graduate School of Medicine, 54 Kawahara-cho, Shogoin, Sakyo-ku, Kyoto 606-8507, Japan. E-mail: ohoto@kuhp.kyoto-u.ac.jp.

RETINAL STRUCTURAL ALTERATIONS AND MACULAR SENSITIVITY IN IDIOPATHIC MACULAR TELANGIECTASIA TYPE 1

KOHEI TAKAYAMA, MD, SOTARO OOTO, MD, HIROSHI TAMURA, MD, KENJI YAMASHIRO, MD, ATSUSHI OTANI, MD, AKITAKA TSUJIKAWA, MD, NAGAHISA YOSHIMURA, MD

Purpose: To evaluate the relationship between the abnormalities of retinal structures showed on spectral-domain optical coherence tomography and the changes in the macular sensitivity measured by microperimetry in eyes with idiopathic macular telangiectasia type 1.

Methods: Eleven eyes of 11 patients with macular telangiectasia type 1 were reviewed. Morphologic changes in the retina and retinal sensitivity of eyes with macular telangiectasia type 1 were studied using spectral-domain optical coherence tomography and microperimetry.

Results: Spectral-domain optical coherence tomographic images revealed disruptions in the photoreceptor inner segment–outer segment (IS/OS) junction in all the eyes and intraretinal cystoid spaces in 10 eyes. In the points that had intraretinal cystoid spaces, the mean retinal sensitivity was 6.8 ± 5.5 dB where the IS/OS was disrupted and 13.4 ± 4.0 dB where the IS/OS was intact ($P < 0.001$). In the points that had intact IS/OS and no cystoid spaces, the mean retinal sensitivity was 15.3 ± 4.3 dB, which was better than that of points that had intact IS/OS with cystoid spaces ($P < 0.001$).

Conclusion: Retinal sensitivity is influenced not only by intraretinal cystoid spaces but also by IS/OS disruptions, and the IS/OS alterations reduce the visual function more severely.

RETINA 0:1–8, 2012

Idiopathic macular telangiectasia (MacTel) is characterized by vascular anomalies affecting the macular capillary network. The term idiopathic juxtafoveolar retinal telangiectasis was first proposed in 1982 by Gass and Oyakawa[1]; in 1993, based on the findings in 140 patients, Gass and Blodi[2] further classified this disease entity. More recently, Yannuzzi et al[3] proposed a simplified classification with 2 distinct types, where type 1 refers to aneurysmal telangiectasia and type 2 to perifoveal telangiectasia.

From the Department of Ophthalmology and Visual Sciences, Kyoto University Graduate School of Medicine, Kyoto, Japan.

Supported in part by a Grant-in-Aid for Scientific Research (21791679) from the Japan Society for the Promotion of Science.

No author has any financial/conflicting interests to disclose.

Reprint requests: Sotaro Ooto, MD, Department of Ophthalmology and Visual Sciences, Kyoto University Graduate School of Medicine, 54 Kawahara-cho, Shogoin, Sakyo-ku, Kyoto 606-8507, Japan; e-mail: ohoto@kuhp.kyoto-u.ac.jp

Typically, patients with MacTel type 1 are men whose mean age at disease onset is 40 years. Gass and Blodi[2] classified this type into two subtypes: Group 1A and 1B. In Group 1A, the telangiectasis is generally confined unilaterally to the temporal half of the macula, occurring in an area of 1 to 2 disk diameters, with equivalent involvement of areas superior and inferior to the horizontal raphe. Macular edema and exudation are the main causes of visual loss in these patients. In Group 1B, the telangiectasia is mainly unilateral and confined to a very small area in 2 clock hours or less at the edge of the foveal avascular zone. However, to date, little information has been available about the relationship between retinal structural abnormalities and visual function in MacTel type 1.

The current study was designed to evaluate the relationship between retinal structures on speckle noise–reduced spectral-domain optical coherence tomography (SD-OCT) and macular sensitivity

measured by microperimetry in eyes with MacTel type 1.

Patients and Methods

This study was a retrospective review of the medical records of 11 male patients (11 eyes) with MacTel type 1 who visited the Macula Service in Kyoto University Hospital, Kyoto, Japan, for the first time between February 2005 and August 2008. The age of patients ranged from 41 to 82 years (mean ± SD, 62.7 ± 12.6 years). The symptoms lasted from 2 weeks to 52 months (median duration, 32 months). All the investigations adhered to the tenets of the Declaration of Helsinki, and the current study was approved by the institutional Review Board and the ethics committee of Kyoto University Graduate School of Medicine.

All the patients had undergone a comprehensive ophthalmologic examination, including measurement of best-corrected visual acuity, intraocular pressure, assessment using indirect ophthalmoscopy and slit-lamp biomicroscopy with contact lens, fundus photography, simultaneous fluorescein angiography, indocyanine angiography with a confocal laser scanning system (HRA2; Heidelberg Engineering, Dossenheim, Germany), and SD-OCT.

MacTel type 1 was diagnosed on the basis of the results of the fundus examination, fluorescein angiography, indocyanine angiography, and optical coherence tomography (OCT) and after exclusion of neovascular maculopathy (i.e., age-related macular degeneration, polypoidal choroidal vasculopathy, retinal angiomatous proliferation, pathologic myopia, idiopathic choroidal neovascularization, and angioid streaks) and other causes of secondary MacTel (i.e., retinal vein occlusion and radiation retinopathy) and diabetes. At the initial visit, all the eyes showed prompt filling of telangiectatic vessels and late intraretinal staining on fluorescein angiography.

SD-OCT: Photoreceptor Layer Features and Retinal Thickness Measurements

Retinal imaging was performed using the Spectralis HRA + OCT (Heidelberg Engineering) at the same visit when microperimetry was performed in all the eyes. First, horizontal and vertical line scans through the fovea centralis were obtained at a 30° angle, followed by 12 radial scans centered at the fovea; finally, volume scans (19 horizontal B-scans at 20° × 30°) were obtained. At each location of interest on the retina, 12 to 50 SD-OCT images were acquired and averaged to reduce speckle noise.

Features of the outer photoreceptor layer of the entire macula on SD-OCT were evaluated by a trained ophthalmologist who was masked to the microperimetry results and other information related to the eyes. A sequence of OCT scans in each data set was examined, and the areas with intraretinal cystoid spaces or disruptions of photoreceptor inner segment–outer segment (IS/OS) junction were identified. As Spectralis HRA + OCT combines confocal scanning laser ophthalmoscopy (SLO) and SD-OCT, it allows the integration of information obtained from SLO fundus image and SD-OCT by pixel to pixel, thus enabling the determination of the exact site of the disrupted IS/OS regions. To exclude the "shadows" of inner retinal changes, such as lipids or intraretinal cystoid spaces, an image-processing program (ImageJ; National Institutes of Health, Bethesda, MD) was used to evaluate the integrity of the IS/OS line. The reflectivity of the IS/OS and the retinal pigment epithelium was measured in ImageJ by using the plot profile function. The IS/OS disruption was defined as the line on the gray-scale image, where the ratio of the IS/OS reflectivity to the retinal pigment epithelium reflectivity had diminished by 2 SD from the reflectivity ratio in the unaffected peripheral macula. Marking an area of interest (i.e., the area with intraretinal cystoid spaces and IS/OS disruption) is performed by manually drawing a line in each B-scan image taken by volume scan (19 horizontal B-scans of 20° × 30°) and projecting it onto the SLO image (Figure 1). Each projected image was then merged into an en-face image (Figure 1). Areas of interest graded in SD-OCT were registered with microperimetric findings (Figure 2).

Retinal thickness was measured on SD-OCT images. B-scan images were analyzed with the built-in software to calculate macular thickness. The values of mean sectorial thickness were displayed in the 9 macular sectors determined by the Early Treatment Diabetic Retinopathy Study (Figure 2).[4] The scans were manually corrected if there were any B-scans with an algorithm failure, such as inaccurately drawn automated boundary lines.

Microperimetry: Retinal Sensitivity Measurements

Fundus-monitored microperimetry was performed with MP-1 (Nidek, Padova, Italy). The MP-1 software contains an automatic tracking system for fundus movements that evaluates every acquired frame for shifts in the directions of the x- and y-axes of the fundus about a reference frame obtained by an infrared camera at the beginning of the examination. A 4-2 staircase strategy with Goldmann size III stimulus was used, and 57 stimulus locations covering the central 20° were examined by microperimetry. The white background illumination was set at 1.27 candela per

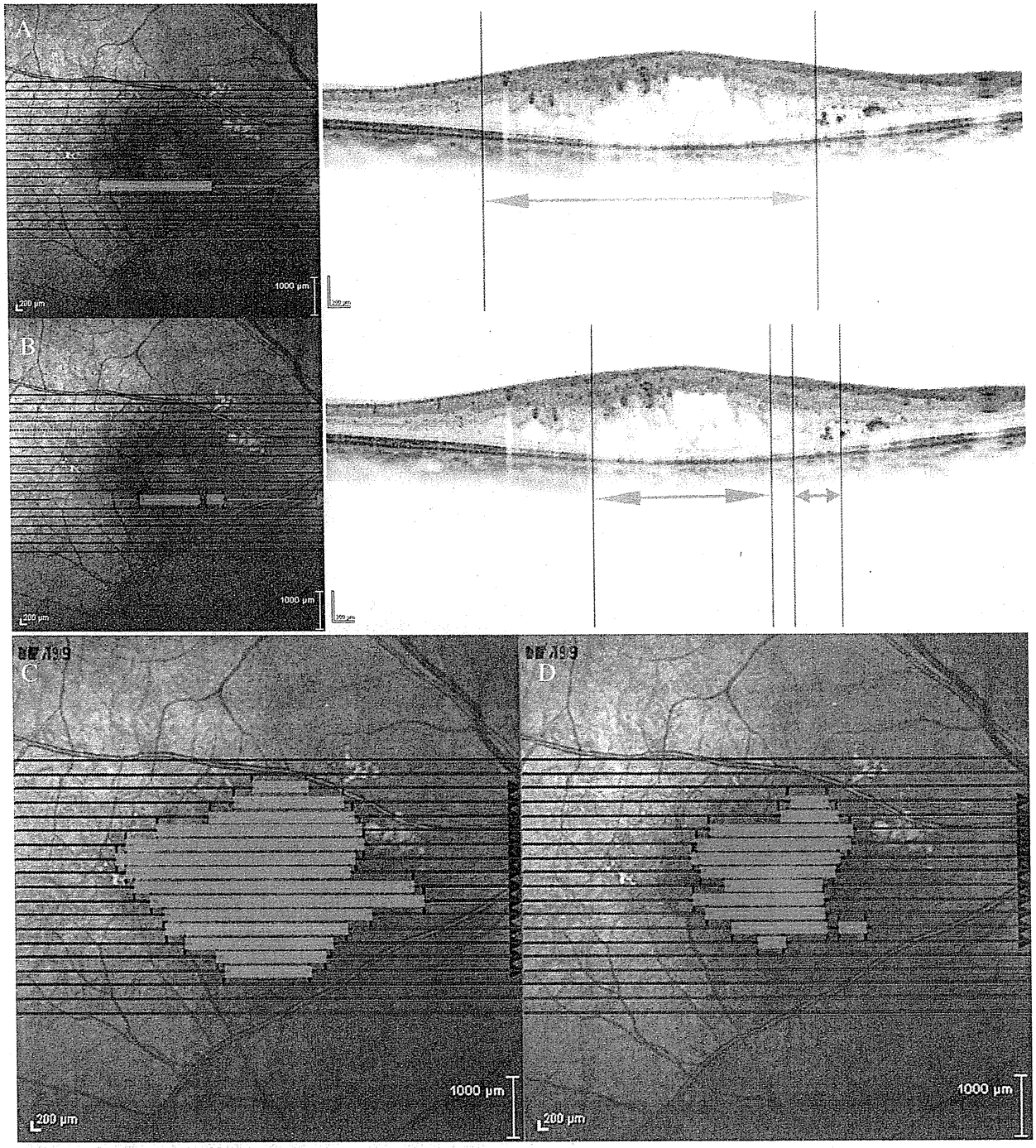

COLOR

Fig. 1. Areas of interest graded in SD-OCT. The SD-OCT imaging protocol comprises 19 B-scans per volume scan of 20° × 30°, and each scan was averaged with 50 frames per B-scan. Marking an area of interest (i.e., the area with intraretinal cystoid spaces [**A**] and disruption of photoreceptor IS/OS junction line [**B**]) is performed by manually drawing a line in each B-scan image and projecting it to the infrared image. Each projection image was merged into one en-face image (**C**, **D**).

square meter (cd/m^2). The differential luminance, defined as the difference between stimulus luminance and background luminance, was 127 cd/m^2 at 0 dB stimulation, and the maximum stimulus attenuation was 20 dB. The duration of the stimulus was 200 ms. After comparing the SLO images obtained by SD-OCT and fundus image obtained by MP-1, the SD-OCT images were registered with the MP-1 images.

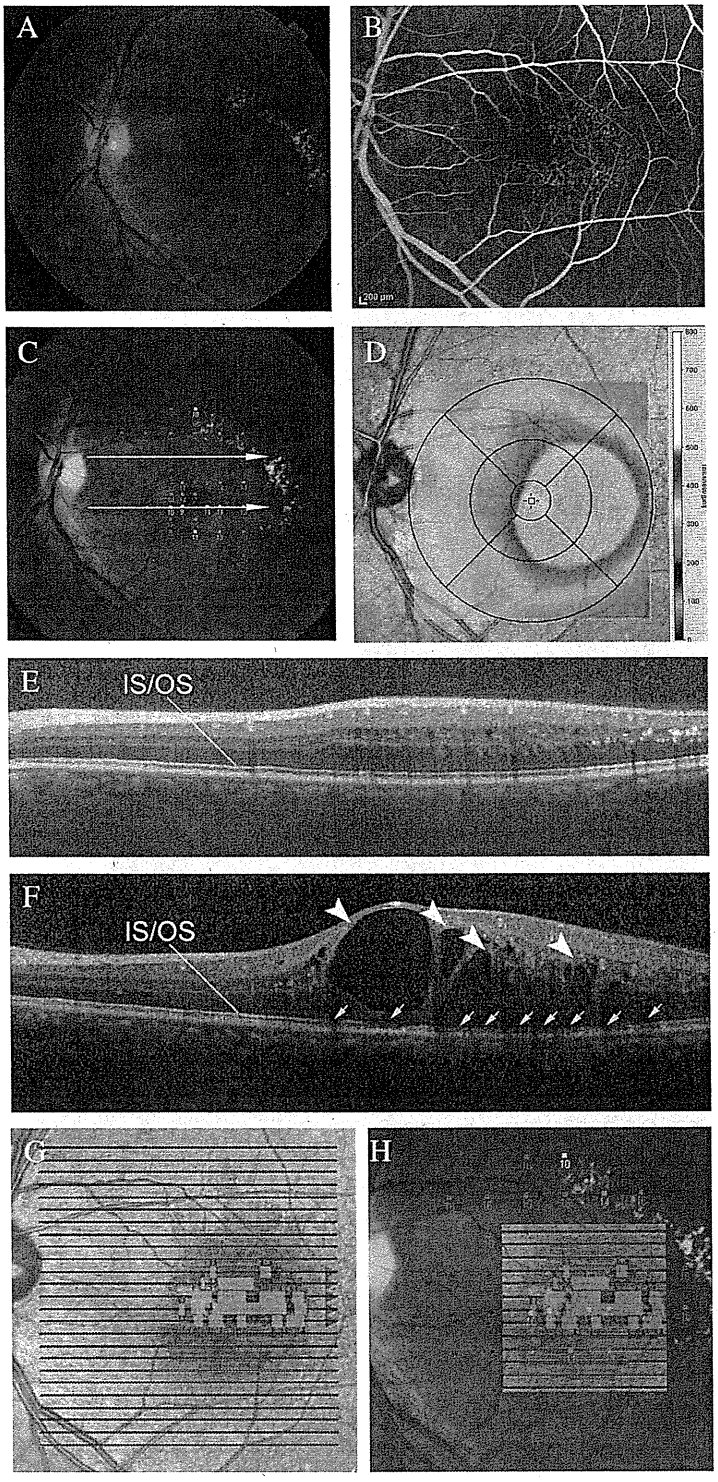

COLOR

Fig. 2. A 55-year-old man had a 6-month history of decreased visual acuity (20/25) and metamorphopsia in the left eye due to idiopathic MacTel type 1. **A**, Fundus photograph showing microaneurysms, cystoid macular edema, and hard exudates. **B**, Fluorescein angiography frame showing telangiectasia and microaneurysms with surrounding leakage. **C**, Retinal sensitivity map, obtained using fundus-monitoring microperimetry, showing decreased sensitivity in the macular area, particularly on the temporal side of the fovea. **D**, Retinal thickness map was generated using SD-OCT, and Early Treatment Diabetic Retinopathy Study layout was overlaid. The area with increased retinal thickness is larger than the area with decreased retinal sensitivity in the microperimetry. **E**, B-scan image of SD-OCT (indicated by upper white arrow in the retinal sensitivity map) showing small intraretinal cystoid spaces and increased retinal thickness but showing an intact photoreceptor IS/OS line. Retinal sensitivity is normal at all measurement points along this scan line. **F**, B-scan image of SD-OCT (indicated by lower white arrow in the retinal sensitivity map) showing intraretinal cystoid spaces (white arrows) and disruptions of the IS/OS line (yellow arrows). Note that retinal sensitivity is severely decreased in the area where the IS/OS is disrupted. **G**, Areas of interest graded in SD-OC: pink = retinal cystoid spaces, orange = IS/OS disruption. **H**, Merged image of microperimetry and areas of interest graded in SD-OCT: pink = retinal cystoid spaces, orange = IS/OS disruption.

Statistical Analysis

The best-corrected visual acuity was measured using a Landolt chart and expressed as a Snellen equivalent or the logarithm of the minimal angle of resolution. Generalized estimating equations (GEEs) were used for the comparison of retinal sensitivity variables. We calculated the Spearman rank correlation coefficient to study associations between retinal sensitivity or visual

acuity and retinal thickness. Because the points in the same eye are not independent, the Mantel–Haenszel test, stratified by eye, was used for comparisons of the retinal sensitivity between points with retinal alterations. The ratios between retinal sensitivity proportions and associated confidence intervals were calculated.[5] All statistical evaluations were performed using a commercially available software program (SPSS 17; SPSS, Inc, Chicago, IL). $P < 0.05$ was considered to be statistically significant.

Results

Fluorescein angiography revealed telangiectasia of the retinal capillaries temporal to the fovea involving approximately one to two disk diameters and leakage from the microaneurysms and telangiectasia. Based on clinical groups proposed by Gass and Blodi,[2] all eyes were classified as Group 1A. Macular edema and lipid deposition were seen in all eyes.

The visual acuity of the affected eyes ranged from 20/100 to 20/15, and the mean logarithm of the minimal angle of resolution visual acuity was 0.245 ± 0.244. Of the 11 eyes studied, 8 (72.7%) had visual acuity of 20/40 or better.

The mean retinal thickness was slightly increased in the temporal sectors as compared with that in nasal sectors, but the difference was not significant ($P = 0.093$ for the inner ring; $P = 0.348$ for the outer ring). The mean retinal thickness correlated with retinal sensitivity ($P = 0.005$, rs = –0.279, Spearman rank correlation coefficient); in particular, the thickness of the inner rings of the Early Treatment Diabetic Retinopathy Study sectors negatively correlated with the mean retinal sensitivity ($P = 0.003$, rs = –0.434, Spearman rank correlation coefficient).

The SD-OCT images revealed disruptions of the photoreceptor IS/OS junction line in a series of OCT sections in all eyes and intraretinal cystoid spaces in 10 of the 11 eyes in this study (Figures 1 and 2). The mean logarithm of the minimal angle of resolution visual acuity of the eyes with disrupted IS/OS lines at the fovea was 0.263 and that of the eyes with intact IS/OS at the fovea was 0.200 ($P = 0.724$).

The SD-OCT findings of disruption in the IS/OS line and the intraretinal cystoid spaces were associated with worse retinal sensitivity (Figures 2–5). Figures 3–5 show the histograms of all measurement points with various retinal sensitivities. At 285 (46.5%) of a total of 613 points, the retinal sensitivity was ≥16 dB. At 254 (56.3%) of 451 points with intact retina, this value was found to be ≥16 dB. However, a retinal sensitivity of ≥16 dB was obtained at only 26 (20.8%) of 126 points with intraretinal cystoid spaces and at 8 (7.4%) of 108 points with disrupted IS/OS line ($P < 0.001$ for both, the Mantel–Haenszel test; Table 1). At points with cystoid spaces, the Mantel–Haenszel risk ratio was 0.33 (95% confidence interval, 0.23–0.47), and at points with IS/OS disruption, the Mantel–Haenszel risk ratio was 6.3 (95% confidence interval, 3.2–12.2).

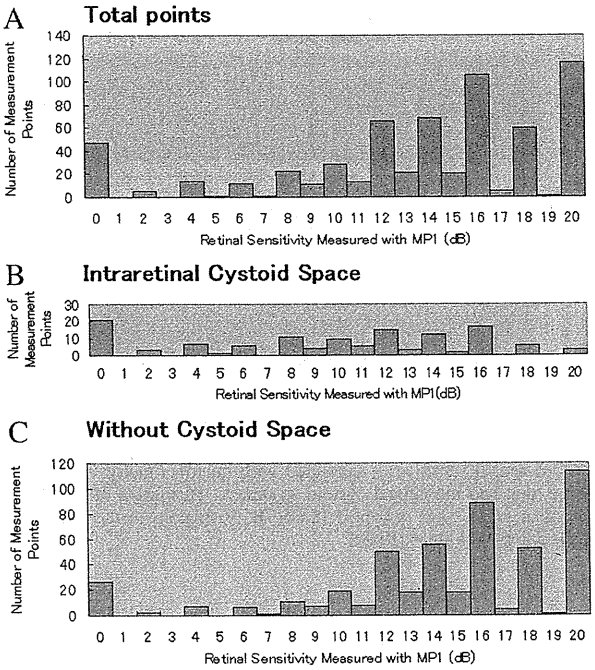

Fig. 3. Histograms showing the numbers of measurement points with various retinal sensitivities measured with microperimetry. **A**, Histogram of all the measurement points. **B**, Histogram of the measurement points with intraretinal cystoid spaces. **C**, Histogram of the measurement points without intraretinal cystoid spaces.

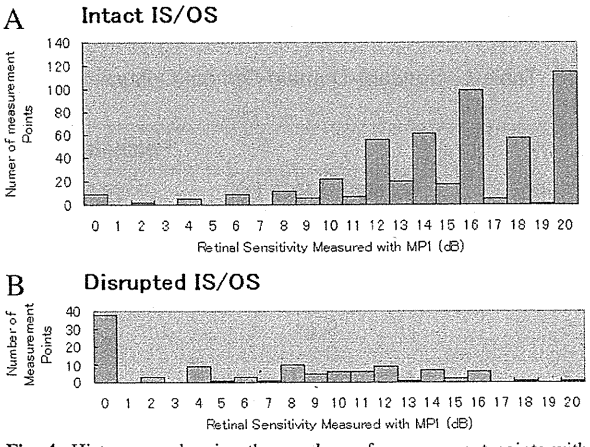

Fig. 4. Histograms showing the numbers of measurement points with various retinal sensitivities measured using microperimetry. **A**, Histogram of the measurement points with intact IS/OS. **B**, Histogram of the measurement points with disrupted IS/OS.

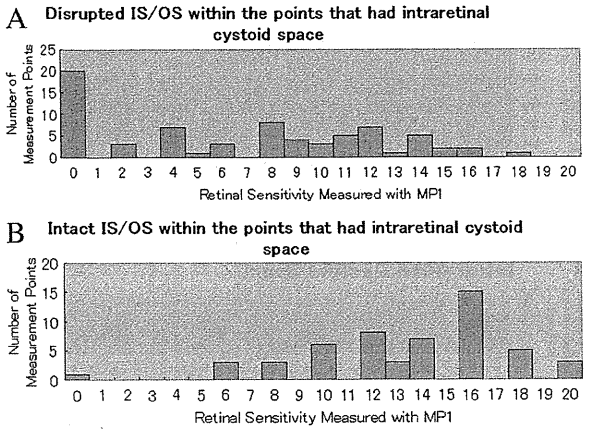

Fig. 5. Histograms showing the numbers of measurement points with various retinal sensitivities measured with microperimetry within the points that had intraretinal cystoid spaces. **A**, Histogram of the measurement points with disrupted IS/OS. **B**, Histogram of the measurement points with intact IS/OS.

However, the retinal sensitivity was ≤10 dB at 141 (23.0%) of 613 points. This value was ≤10 dB only at 53 (11.8%) points with intact retinas. However, a retinal sensitivity of ≤10 dB was obtained at 62 (49.2%) of 126 points with intraretinal cystoid spaces and at 75 (69.4%) of 108 points with disrupted IS/OS line ($P <$ 0.001 for both, the Mantel–Haenszel test). At points with cystoid spaces, the Mantel–Haenszel risk ratio was 6.2 (95% confidence interval, 4.0–9.5), and at points with IS/OS disruption, the Mantel–Haenszel risk ratio was 0.21 (95% confidence interval, 016–0.28).

The mean retinal sensitivity was 9.6 ± 5.9 dB at the points with intraretinal cystoid spaces and 14.5 ± 5.1 dB at the points without them ($P <$ 0.001, GEE; Table 2). The mean retinal sensitivity was 15.1 ± 4.3 dB at the points with intact IS/OS and 6.4 ± 5.9 dB with disrupted IS/OS ($P <$ 0.001, GEE; Table 2). Within the points that had intraretinal cystoid spaces, the mean retinal sensitivity was 6.8 ± 5.5 dB where the IS/OS was disrupted and 13.4 ± 4.0 dB where the IS/OS was intact ($P <$ 0.001, GEE). Within the points that had intact IS/OS and no cystoid spaces, the mean retinal sensitivity was 15.3 ± 4.3 dB, which was better than that of points that had intact IS/OS with cystoid spaces ($P <$ 0.001, GEE).

Discussion

Previous studies using time-domain OCT images obtained in eyes with MacTel type 1 revealed structural abnormalities in the macula, such as intraretinal cystoid spaces, retinal thickening, and macular detachment.[3] However, since these observations were based on conventional time-domain OCT, further interpretation of the structural change in the photoreceptors is difficult. The autotracking function of the MP-1 corrects for shifts in the measurement position because of small involuntary movements, thereby allowing more accurate measurement of retinal sensitivity with the certainty of knowing the exact site of origin. In addition, by using an eye tracking system, the Spectralis HRA + OCT system has solved the problem of motion artifacts that limit the confident detection of small changes, which permits the production of detailed, speckle noise–reduced images of all the retinal layers. Our study was the first to identify, by using speckle noise–reduced SD-OCT and microperimetry, structural abnormalities in the macula and correlations between this anatomical finding and the retinal sensitivity in eyes with MacTel type 1.

Visual acuity has been reported to be usually 20/40 or better in eyes with MacTel type 1.[1–3] In the current study, 8 of the 11 eyes investigated had visual acuity

Table 1. Spectral-Domain Optical Coherence Tomographic Findings and Percentage of Points With Retinal Sensitivities ≥16 dB

	Percentage of Points With Retinal Sensitivities ≥16 dB			
Patient	Cystoid Space (+)	Cystoid Space (–)	IS/OS Disruption (+)	IS/OS Disruption (–)
1	44.0	90.6	8.3	86.7
2	0	97.7	0	97.7
3	16.7	15.7	16.7	15.4
4	0	19.6	0	22.7
5	9.1	69.6	18.2	67.4
6	0	17.9	28.6	16.0
7	60.0	85.1	0	80.7
8	25.0	62.1	0	68.6
9	0	21.4	0	18.4
10	4.2	57.6	0	50.0
11	None*	73.7	0	73.7

*None: there were no points with cystoid space.

Table 2. Relationship Between SD-OCT Findings and Mean Retinal Sensitivity on Microperimetry

	Retinal Sensitivity (dB)
Cystoid space (+)	9.6 ± 5.9
Cystoid space (–)	14.5 ± 5.1
IS/OS disruption (+)	6.4 ± 5.9
IS/OS disruption (–)	15.1 ± 4.3

of 20/40 or better. Although visual acuity reflects only foveal function, MP-1 enabled the evaluation of function not only in the fovea but also in the larger macular area and is thus of great value for evaluation of the pathologic condition underlying the functional disturbance. Retinal sensitivity of ≥16 dB was obtained in 46.5% of the measurement points in eyes with MacTel type 1. However, 23.0% of measurement points showed a retinal sensitivity of ≤10 dB. These results suggest that despite keeping good visual acuity, some of the eyes with MacTel type 1 had focal areas of decreased retinal function.

Several reports have shown the relationship between retinal thickness and retinal sensitivity in various diseases that cause macular edema. Vujosevic et al[6] reported a negative correlation between macular sensitivity and retinal thickness in eyes with diabetic macular edema. Yamaike et al[7] reported negative correlation between retinal thickness and retinal sensitivity in eyes with retinal vein occlusion. In the current study, the mean retinal thickness of the inner rings of Early Treatment Diabetic Retinopathy Study sectors negatively correlated with the mean retinal sensitivity. Moreover, the areas with intraretinal cystoid spaces showed reduced retinal sensitivity. These results suggest that cystoid macular edema has a relationship with poor visual function in eyes with MacTel type 1; this finding is identical to that in other diseases causing cystoid macular edema.

Retinal sensitivity correlates with retinal structural alterations. In the current study, the area with disrupted IS/OS or intraretinal cystoid spaces showed significantly reduced retinal sensitivity. In addition, the areas with disrupted IS/OS showed significantly reduced retinal sensitivity than those with intact IS/OS, even within the areas having intraretinal cystoid spaces. These results suggest that retinal sensitivity may be influenced not only by intraretinal cystoid spaces but also by IS/OS disruptions, and the IS/OS alterations, which are more closely related to photoreceptor damages, reduce the visual function more severely. The changes in intraretinal microangiopathy were evident in the superficial and deep circulations with leakage into the retina and cystoid macular edema, which may cause photoreceptor damages. Thus, vision impairment in MacTel type 1 may be related mainly to photoreceptor alterations following cystoid macular edema caused by vascular leakage.

Several studies on other diseases have examined the relationship between retinal sensitivity and structural abnormality.[8,9] In resolved central serous retinopathy,[8] at 80% of points with intact IS/OS, retinal sensitivity was ≥16 dB, whereas this sensitivity was only obtained in 20% of points with disrupted IS/OS. The mean retinal sensitivities within the area with disrupted IS/OS were 11.5 dB. In the current study, at 56% of points with an intact retina, retinal sensitivity was ≥16 dB, whereas this sensitivity was only obtained in 20% of points with cystoid spaces and in 7% of points with disrupted IS/OS. The mean retinal sensitivities within the area with disrupted IS/OS were 6.4 dB. These results suggest that decreased retinal sensitivity in areas with disrupted IS/OS is a common phenomenon in these retinal diseases.

There have been several reports on the assessment of microperimetry with MacTel type 2.[9–14] Charbel Issa et al[10] reported that macular sensitivity significantly decrease temporal to the fovea and light increment sensitivity deteriorates in eyes at more severe stages. Another study also reported that central light sensitivity in eyes with nonproliferative type 2 MacTel with normal central foveal thickness was lower than that in eyes with subnormal central foveal thickness.[11] Schmitz-Valckenberg et al[12] reported that severe reduction in retinal sensitivity is spatially confined to morphologic alterations seen with SLO imaging. Maruko et al[14] reported a reduction in the retinal sensitivity thresholds temporal to the fovea, particularly in the area of IS/OS breaks and the area of right angle vein corresponding to the disappearance of the outer retinal layer. Thus, photoreceptor alterations are likely to be associated with retinal sensitivity both in type 1 and type 2 MacTel, although it has been postulated that the pathophysiology between the 2 types of MacTel may be considerably different.[1–3,15]

In conclusion, SD-OCT with reduced speckle noise allows detailed observation of retinal structures and thus helps to evaluate the relationship between retinal structural abnormalities and visual function. Limitations of the current study include its retrospective nature and small sample size. Another limitation of this study is that the symptom duration varied greatly, that is, from 2 weeks to 52 months, and this might have an impact on the comparisons. However, our findings suggest that the IS/OS disruptions are one of the most important factors affecting retinal function in eyes with MacTel type 1.

Key words: idiopathic macular telangiectasia, microperimetry, retinal structure, photoreceptor inner and outer segment junction line, optical coherence tomography.

Acknowledgment

The authors thank Toshiya Sato (Professor, Department of Biostatistics, Kyoto University Graduate School of Medicine) for assisting in statistical analysis.

References

1. Gass JD, Oyakawa RT. Idiopathic juxtafoveolar retinal telangiectasis. Arch Ophthalmol 1982;100:769–780.
2. Gass JD, Blodi BA. Idiopathic juxtafoveolar retinal telangiectasis. Update of classification and follow-up study. Ophthalmology 1993;100:1536–1546.
3. Yannuzzi LA, Bardal AM, Freund KB, et al. Idiopathic macular telangiectasia. Arch Ophthalmol 2006;124:450–460.
4. Early photocoagulation for diabetic retinopathy. ETDRS report number 9. Early Treatment Diabetic Retinopathy Study Research Group. Ophthalmology 1991;98:766–785.
5. Sato T. Confidence limits for the common odds ratio based on the asymptotic distribution of the Mantel-Haenszel estimator. Biometrics 1990;46:71–80.
6. Vujosevic S, Midena E, Pilotto E, et al. Diabetic macular edema: correlation between microperimetry and optical coherence tomography findings. Invest Ophthalmol Vis Sci 2006;47:3044–3051.
7. Yamaike N, Kita M, Tsujikawa A, et al. Perimetric sensitivity with the micro perimeter 1 and retinal thickness in patients with branch retinal vein occlusion. Am J Ophthalmol 2007;143:342–344.
8. Ojima Y, Tsujikawa A, Hangai M, et al. Retinal sensitivity measured with the micro perimeter 1 after resolution of central serous chorioretinopathy. Am J Ophthalmol 2008;146:77–84.
9. Ooto S, Hangai M, Takayama K, et al. High-Resolution Photoreceptor Imaging in Idiopathic Macular Telangiectasia Type 2 Using Adaptive Optics Scanning Laser Ophthalmoscopy. Invest Ophthalmol Vis Sci 2011;52:5541–5550.
10. Charbel Issa P, Helb HM, Rohrschneider K, et al. Microperimetric assessment of patients with type 2 idiopathic macular telangiectasia. Invest Ophthalmol Vis Sci 2007;48:3788–3795.
11. Charbel Issa P, Helb HM, Holz FG, et al. Correlation of macular function with retinal thickness in nonproliferative type 2 idiopathic macular telangiectasia. Am J Ophthalmol 2008;145:169–175.
12. Schmitz-Valckenberg S, Fan K, Nugent A, et al. Correlation of functional impairment and morphological alterations in patients with group 2A idiopathic juxtafoveal retinal telangiectasia. Arch Ophthalmol 2008;126:330–335.
13. Schmitz-Valckenberg S, Ong EE, Rubin GS, et al. Structural and functional changes over time in MacTel patients. Retina 2009;29:1314–1320.
14. Maruko I, Iida T, Sekiryu T, Fujiwara T. Early morphological changes and functional abnormalities in group 2A idiopathic juxtafoveolar retinal telangiectasis using spectral domain optical coherence tomography and microperimetry. Br J Ophthalmol 2008;92:1488–1491.
15. Takayama K, Ooto S, Tamura H, et al. Intravitreal bevacizumab for type 1 idiopathic macular telangiectasia. Eye 2010;24:1492–1497.